Journal of Applied Physics

# Elastic properties of single crystal hydrogen sulfide: A Brillouin scattering study under high pressure-temperature

Cite as: J. Appl. Phys. **124**, 125901 (2018); https://doi.org/10.1063/1.5040399
Submitted: 17 May 2018 . Accepted: 31 August 2018 . Published Online: 25 September 2018

Di Zhou, Xiaoli Huang, Xin Li, Hongyu Yu, Fangfei Li, Yanping Huang, Mengya Lu, Yongfu Liang, Mingkun Liu, Gang Wu, Qiang Zhou, Bingbing Liu, and Tian Cui

AIP Publishing

JOURNAL OF APPLIED PHYSICS **124**, 125901 (2018)

# Elastic properties of single crystal hydrogen sulfide: A Brillouin scattering study under high pressure-temperature

Di Zhou, Xiaoli Huang,[a] Xin Li, Hongyu Yu, Fangfei Li, Yanping Huang, Mengya Lu,
Yongfu Liang, Mingkun Liu, Gang Wu, Qiang Zhou, Bingbing Liu, and Tian Cui[a]
*State Key Laboratory of Superhard Materials, College of Physics, Jilin University, Changchun 130012,*
*People's Republic of China*

(Received 17 May 2018; accepted 31 August 2018; published online 25 September 2018)

We have performed high pressure-temperature Brillouin scattering measurements on single crystal hydrogen sulfide using externally heated diamond anvil cell techniques. The pressure dependences of the acoustic velocities, isothermal elastic constants, and moduli of single crystal hydrogen sulfide have been determined along four isotherms. Both elastic constants and moduli increase monotonously with pressure along each isotherm, while they show a decreased tendency with temperature elevated under the same pressure points. The experimental equation of state of single crystal hydrogen sulfide is obtained by fitting with a third-order Birch-Murnaghan and Tait equation. It is proposed that the effect of hydrogen bonds contributes to the unique tendency of elastic anisotropy in single crystal hydrogen sulfide. Through our work, we have extended the melting curve and phase diagram of hydrogen sulfide up to 12 GPa and 580 K. *Published by AIP Publishing.*
https://doi.org/10.1063/1.5040399

## I. INTRODUCTION

Hydrogen-rich compounds are not only potential high-temperature superconductors,[1–5] but also promising hydrogen storage materials.[6,7] However, multiple attempts to find a material with high critical superconducting temperature in hydrogen-rich compounds did not produce a high-$T_c$ material. Until recently, the superconducting critical temperature of $H_3S$ has been discovered up to 200 K at high pressure in both theory[8,9] and experiment,[10,11] which breaks the previous record of a copper base superconductor with 164 K[12] and further stimulates the research upsurge about high pressure behavior of hydrogen chalcogenide.[13–16] It is reported that $H_3S$ can be obtained by pressurized hydrogen sulfide ($H_2S$) directly.[8,13,17] A high pressure-temperature ($P$-$T$) equation of state (EOS) is the basis of studying the structures and properties of materials and has important significance to understand the mechanism of phase transformation. Based on this, the study of EOS on $H_2S$ is helpful to understand its decomposition process and phase transitions.

$H_2S$ is quite a typical molecule with hydrogen bonding and is known to show three solid phases with increasing temperature at ambient pressure.[18] The lowest-temperature phase III below 103.5 K is orientation ordered and has orthorhombic $Pbcm$ or tetragonal $P4_2$ with a unit cell containing 16 molecules, and each molecule with its neighbors forms a quasi-two-dimensional hydrogen-bonded network.[19] Middle phase II from 103.5 to 126.2 K has the space group $Pa\bar{3}$ with four molecules in the unit cell, and each molecule randomly flips by breaking and remaking of temporary hydrogen bonds.[18,20] High temperature phase I is stable between 126.2K and 187.6 K. This plastic phase is an orientation disordered face-centered cubic structure with space group $Fm\bar{3}m$, where the disordered S–H bond orientations are isotropic or pseudo-isotropic.[21] The solid phase I maintained from 0.47 to 8 GPa at 300 K, and then the phase I transforms to I′, which is simple primitive cubic and has space group $P2_13$. After 11 GPa, the transition from cubic phase I′ to the lower symmetrical phase IV is still controversial.[22–25] Until now, the present phase diagram of $H_2S$ is limited to room temperature and low temperature. Brillouin scattering is a convenient method applied to high pressure experiments due to the transparency of diamond.[26] It provides precise elastic properties and valuable information on the atomic interaction of materials under pressure to better understand the phase transition mechanism. Previously, Shimizu and co-workers have measured the angular dependence of Brillouin frequency in crystalline $H_2S$ up to 7 GPa at room temperature[27] and 3.7 GPa at 240 K.[28]

In this work, we complete high-temperature data information and provide a thorough characterization of high $P$-$T$ elasticity in $H_2S$. We obtain single crystal $H_2S$ under high pressure at four temperatures successfully and perform the velocity measurements on the single crystal sample by the Brillouin scattering method. The elastic properties and isothermal moduli of $H_2S$ are derived with identification of its crystal orientation.

## II. EXPERIMENTAL DETAILS

In an argon atmosphere glovebox, commercial gaseous $H_2S$ with purity above 99.999% is loaded into standard symmetric diamond anvil cell (DAC) for room temperature and BX90 DAC for high temperature measurements with tungsten gaskets. All tubes from the lecture bottle to the DAC are firstly purged of $H_2S$ gas to minimize the contaminations. The $H_2S$ sample is condensed below 170 K by spraying its vapor into the gasket holes (diameter 180 $\mu$m, depth 50-60 $\mu$m) of a DAC cooled in a liquid nitrogen bath. The

---

[a] Authors to whom correspondence should be addressed: huangxiaoli@jlu.edu.cn and cuitian@jlu.edu.cn

targeted single crystal is grown from a seed crystal after recovering to room temperature. A small ruby chip in sample chamber is used for pressure measurement, and a resistance heater is fixed around the DAC by high temperature cement. The temperature of the sample is determined by a K-type thermocouple, which is glued to the side of diamond with cement and controlled by a feedback power holding a fluctuation within 1 K. Because of the existence of temperature gradient around the sample chamber, the temperature dispersion between anvil center and side face of the diamond cannot be ignored. To obtain the accurate temperature of the sample chamber, the calibrated curve is calibrated for each high *P-T* DAC before Brillouin scattering measurements.

Room temperature *in situ* Brillouin scattering and synchrotron X-ray diffraction (XRD) experiments are performed at APS-Beamline 13 BM-D. The scattering angle of the on-line Brillouin system is 50°. The wavelength of the X-ray is 0.3344 Å, and focused X-ray spot is 14 $(H) \times 4$ $(V)$ $\mu m^2$.[29] High temperature Brillouin measurements are performed using a custom-built Brillouin system with a 3 + 3 pass tandem Fabry–Perot interferometer. The symmetric platelet 60° is used for high temperature experiments. Both two Brillouin systems use 532 nm as excitation source.

## III. RESULTS AND DISCUSSION

### A. Brillouin scattering spectra and sound velocity

The high pressure Brillouin scattering spectra of $H_2S$ are collected along four isotherms: 300, 400, 500, and 580 K. The measured data points from this work are shown in Fig. 1 together with literature data. The phase diagram of $H_2S$ is extended up to 580 K. The measured highest pressure along each isotherm is up to respective pressure points where the transverse modes could not be detected (except 500 K), which might be because of the shattering of single crystal. This is consistent with the appearance of diffraction ring in the red block region shown in Figs. 2(c) and 2(d). At platelet scattering geometry, the wave vectors of observed phonons are parallel to the inner face of the diamond anvil, and the Brillouin shifts are independent of the refractive index. The Brillouin frequency shift $(\Delta\upsilon)$ is related to sound velocity $(v)$ using the equation:

$$v = \frac{\lambda_0 \Delta\upsilon}{2\sin\left(\frac{\theta}{2}\right)}, \tag{1}$$

where $\lambda_0$ is the incident laser wavelength and scattering angle $\theta$ is 50° or 60° in this experiment.

At 300 K, a seed crystal coexists with liquid at about 0.67 GPa, and the photo of the sample chamber is shown in Fig. 2(a), where the right circle around ruby is the seed crystal. After the crystal is fully grown, XRD spectra are measured to confirm single crystal in the DAC. The typical diffraction points presented in Fig. 2(b) prove a high-quality single crystal. Figure 3 shows representative Brillouin spectra of $H_2S$ under high pressures at 300 K and 500 K. We obtain the longitudinal signal of liquid phase; meanwhile, a pair of backscattering $(\Delta\nu_{180°})$ signal is detected caused by incident light reflecting from the output diamond anvil serves as backscattering incident light [see Fig. 3(b)]. All three modes (LA, $TA_1$, and $TA_2$) are measured after crystalizing at 0.84 GPa and 300 K. For 500 K isotherm, after solidification at 1.71 GPa, both longitudinal and transverse acoustic modes of the target can be detected. It can be seen that Brillouin peaks shift fast with pressure along these two isotherms. Pressure has more obvious effect on the decreased intensity than temperature. Besides, the shattering of single crystal greatly

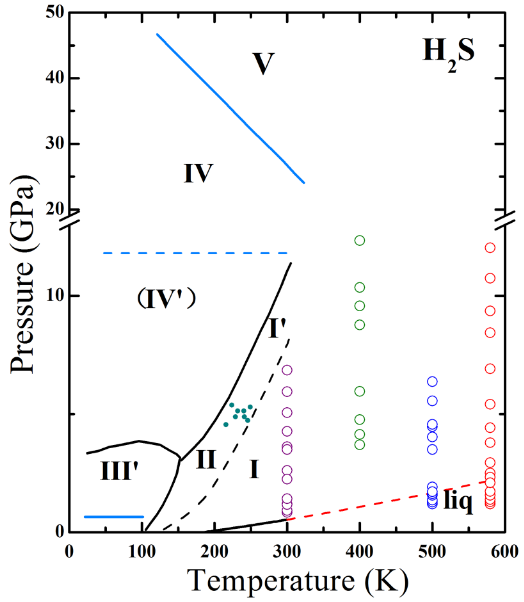

FIG. 1. The pressure-temperature phase diagram of $H_2S$. The black curves are phase boundaries determined by Raman experiments.[30] Blue lines are from Fujihisa *et al.* by XRD experiments.[31] Cyan points between I′ and II are determined by neutron experiments.[32] The red dashed lines between liquid and I are determined in this work. The measured pressure points of four isotherms labeled by hollow circles are also given in the figure.

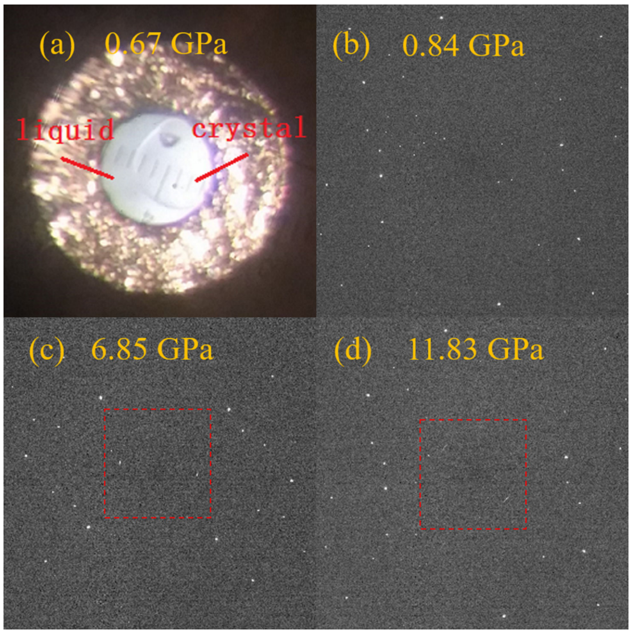

FIG. 2. (a) The photo of the sample chamber at 0.67 GPa and 300 K. Room temperature X-ray diffraction (XRD) 2D images of the sample at (b) 0.84 GPa, (c) 6.85 GPa, and (d) 11.83 GPa, respectively.

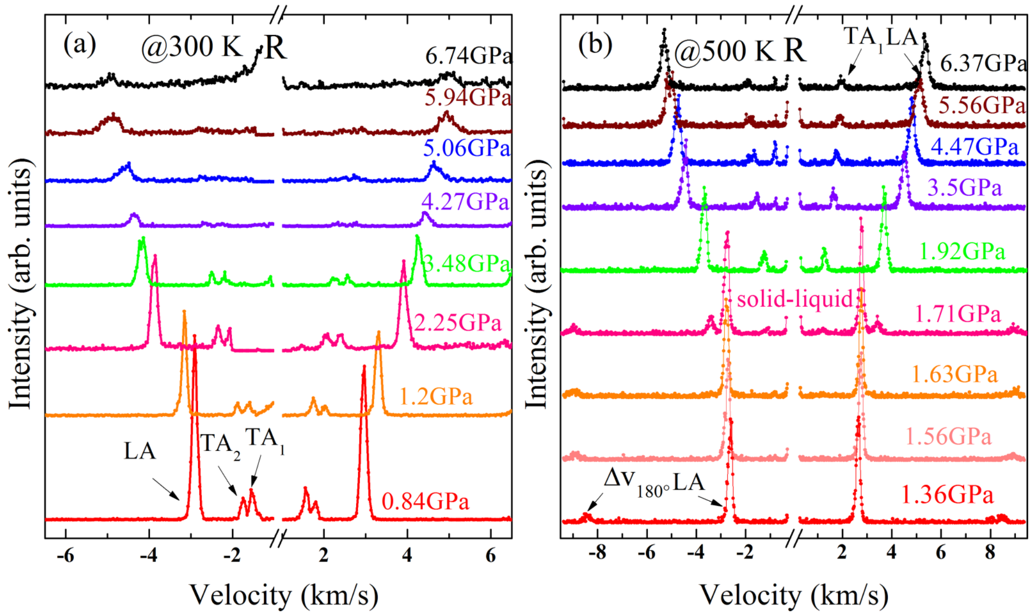

FIG. 3. Brillouin scattering spectra of $H_2S$ under high pressures at (a) 300 K and (b) 500 K with the azimuthal angle $\varphi = 170°$. R refers to the Rayleigh scattering; LA, $TA_1$, and $TA_2$ represent the longitudinal mode, slow transverse mode, and fast transverse mode, respectively, $\Delta\nu_{180°}$ is the backscattering signal.

affects the decrease on intensity, and the obvious broadening of LA peaks at higher pressure. Our measured pressure just reaches 6.37 GPa along 500 K because of the heater oxidation and melting of the resistance wire.

In the present study, liquid $H_2S$ firstly solidifies into phase I: an orientation disordered face-centered cubic structure with space group $Fm\bar{3}m$. Three independent elastic constants are needed to fully describe the elastic behavior of

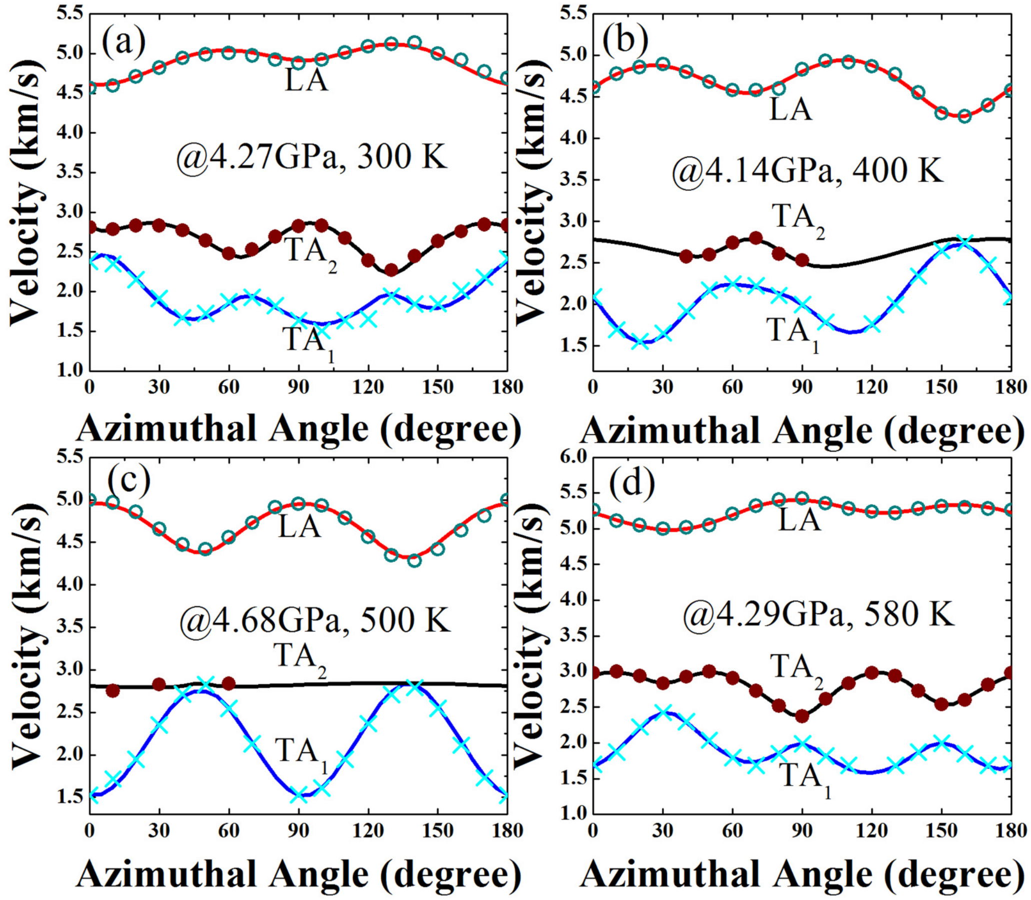

FIG. 4. Acoustic velocity of LA, $TA_1$, and $TA_2$ modes as a function of angle $\varphi$ measured in platelet geometry for the crystalline $H_2S$: (a) $P = 4.27$ GPa, $T = 300$ K, (b) $P = 4.14$ GPa, $T = 400$ K, (c) $P = 4.68$ GPa, $T = 500$ K, and (d) $P = 4.29$ GPa, $T = 580$ K. Green, red, and cyan symbols indicate experimental points LA, $TA_2$, and $TA_1$, respectively; and the red, black, and blue solid curves are calculated using best-fit elastic constants, respectively.

TABLE I. Isothermal bulk modulus and its pressure derivative determined from two EOS forms along four isotherms.

| | Tait | | | Third-order B-M | | |
|---|---|---|---|---|---|---|
| | $B_0$ (GPa) | $B'_0$ | $V_0$ ($cm^3$/g) | $B_0$ (GPa) | $B'_0$ | $V_0$ ($cm^3$/g) |
| 300 K | 3.85 (4) | 6.23 (1) | 0.88 (5) | 4.93 ± 2.21 | 5.04 ± 1.1 | 0.88 (4) |
| 400 K | 3.4 (2) | 6.1 (1) | 0.92 (3) | 5.72 ± 1.09 | 4.57 ± 0.33 | 0.88 (2) |
| 500 K | 3.31 (1) | 5.69 (5) | 0.95 (4) | 5.75 ± 0.69 | 4.15 ± 0.17 | 0.92 (2) |
| 580 K | 3.3 (8) | 5.8 (4) | 0.99 (2) | 3.29 ± 1.13 | 5.26 ± 0.57 | 1.00 (5) |

cubic structure, that is, longitudinal constant $C_{11}$, shear constants $C_{44}$, and the off-diagonal constants $C_{12}$. On the basis of the theory developed by Every,[33] the angle dependence of acoustic velocities can be measured by rotating the DAC about the axis perpendicular to the culet of the diamond with 10° intervals[34] (±0.2°). Then, according to Christoffel's equation of cubic crystal, the acoustic modes can be expressed as follows:

$$\rho v_j^2 = f_j(C_{11}, C_{12}, C_{44}, \ \theta, \varphi, \chi), \tag{2}$$

where $\rho$ is the density; the subscript $j$ (=0, 1, 2) indicates one longitudinal (L) and two transverse modes ($TA_1$ and $TA_2$), respectively; $C_{ij}$ is the adiabatic elastic constant; and the Euler angles ($\theta$, $\varphi$, $\chi$) relate the crystal reference frame to the laboratory frame. Then, a least-squares fit between the calculated $f_j(\varphi_i)$ as a function of experimental velocities ($\varphi_i$, $v_{ji}$) is performed:

$$R = \sum\nolimits_{ij} [f_j(\varphi_i) - v_{ji}]^2, \quad j = 0, 1, 2. \tag{3}$$

The azimuthal angle $\varphi$ is the only variable during measurement. The sum of square errors $R$ is minimized by systematically varying all of the parameters until the fit is optimized. As a result, three ratios of elastic constants to density ($C_{11}/\rho$, $C_{12}/\rho$, and $C_{44}/\rho$) and the crystal orientation can be determined completely. The crystallographic axes of a single crystal grown in the DAC can be determined by XRD. However, at high temperature, we identify the crystal orientation ($\theta$, $\varphi$, $\chi$) under each applied pressure only by using Brillouin scattering spectra as the method described above.

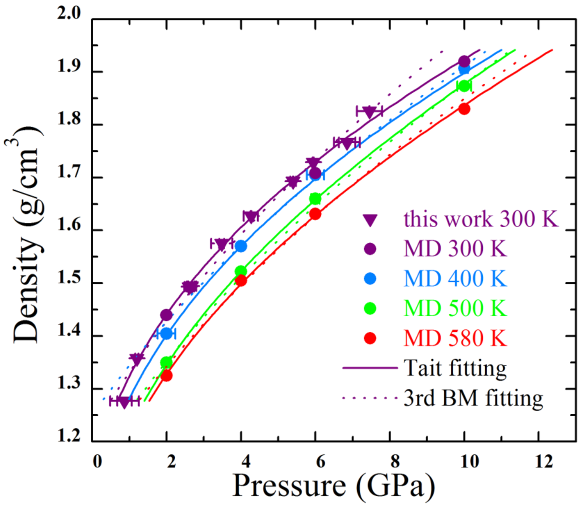

FIG. 5. Density variation with pressure for $H_2S$ at four isotherms: 300, 400, 500, and 580 K, respectively. Solid and dotted lines are best-fitted results using Tait and third-order BM EOS. Down triangle symbols represent XRD data of this work, and solid circle symbols are the calculated values at high temperature.

In Fig. 4, the velocities of LA, $TA_1$, and $TA_2$ modes as a function of angles $\varphi$ around 4 GPa are presented at different temperatures together with solid curves calculated from best-fit elastic constants. Obviously, the acoustic velocities of single crystal $H_2S$ exhibit highly anisotropic, and this character maintains in all experimental $P$-$T$ range. The crystal orientation at 500 K is different from the other isotherms since this crystal grows at 500 K while others are at ambient temperature. Theoretical research studies prove that the acoustic modes would appear or disappear in a certain scattering geometry.[35] As shown in Figs. 4(b) and 4(c), we can observe only one slow shear mode $TA_1$ for most azimuthal angle, and the intensity of this mode varies little with the phonon direction changing in rotation plane.

## B. Equation of state

Considering there are no high-temperature density data of $H_2S$, we adopt *ab initio* molecular dynamics (MD) simulations in the Vienna *ab initio* simulation package (VASP) code[36–38] to investigate $H_2S$. The projector-augmented wave (PAW) method[39,40] and the Perdew-Burke-Ernzerhof generalized gradient approximation (GGA)[41] for exchange-correlation functions are used. Monkhorst-Pack k-point with 2 × 2 × 2 mesh[42] and the cutoff energy with 400 eV are set. Simulations are implemented in a constant number of particles, pressure, and temperature ensemble[43] for a system containing 64 $H_2S$ molecules. Then, we try to fit the relationship among volume, pressure, and temperature with Tait and third-order Birch-Murnaghan EOS as follows:

$$P = \frac{B_0}{(B'_0 + 1)} \left\{ \exp\left[ (B'_0 + 1)\left(1 - \frac{V}{V_0}\right) \right] - 1 \right\}, \tag{4}$$

$$P = \frac{3B_0}{2} \left[ \left(\frac{V_0}{V}\right)^{\frac{7}{3}} - \left(\frac{V_0}{V}\right)^{\frac{5}{3}} \right] \times \left\{ 1 + \frac{3}{4}(B'_0 - 4) \left[ \left(\frac{V_0}{V}\right)^{\frac{2}{3}} - 1 \right] \right\}, \tag{5}$$

TABLE II. The values of $C_{ij}/\rho$ (GPa × cm$^3$/g) together with the calculated density ρ at each *P* (GPa)-*T* (K) conditions.

| 300 K | | | | | 400 K | | | | |
|---|---|---|---|---|---|---|---|---|---|
| Pressure | ρ | $C_{11}/\rho$ | $C_{12}/\rho$ | $C_{44}/\rho$ | Pressure | ρ | $C_{11}/\rho$ | $C_{12}/\rho$ | $C_{44}/\rho$ |
| 0.84 | 1.28 | 9.16 | 6.70 | 3.98 | 3.70 | 1.55 | 20.19 | 14.94 | 8.45 |
| 0.92 | 1.30 | 9.41 | 7.09 | 4.05 | 4.14 | 1.58 | 20.15 | 15.19 | 8.78 |
| 1.17 | 1.34 | 10.52 | 7.81 | 4.66 | 4.77 | 1.62 | 21.99 | 16.42 | 9.69 |
| 1.20 | 1.35 | 11.15 | 8.36 | 4.94 | 5.95 | 1.69 | 25.35 | 18.40 | 10.94 |
| 1.42 | 1.36 | 12.20 | 9.10 | 5.38 | 8.77 | 1.85 | 30.90 | 22.88 | 12.90 |
| 2.25 | 1.45 | 15.36 | 11.41 | 6.74 | 9.57 | 1.90 | 33.26 | 24.49 | 13.46 |
| 2.61 | 1.49 | 15.83 | 11.84 | 6.94 | 10.36 | 1.91 | 33.25 | 23.46 | 13.86 |
| 3.50 | 1.56 | 18.94 | 14.17 | 8.43 | 12.34 | 1.95 | 37.12 | 26.31 | 13.74 |
| 3.62 | 1.58 | 19.44 | 14.35 | 8.35 | | | | | |
| 4.27 | 1.63 | 20.97 | 15.56 | 9.28 | | | | | |
| 5.06 | 1.69 | 23.89 | 17.17 | 9.70 | | | | | |
| 5.94 | 1.73 | 25.12 | 18.10 | 10.65 | | | | | |
| 6.85 | 1.77 | 26.48 | 18.05 | 10.74 | | | | | |

| 500 K | | | | | 580 K | | | | |
|---|---|---|---|---|---|---|---|---|---|
| Pressure | ρ | $C_{11}/\rho$ | $C_{12}/\rho$ | $C_{44}/\rho$ | Pressure | ρ | $C_{11}/\rho$ | $C_{12}/\rho$ | $C_{44}/\rho$ |
| 1.92 | 1.33 | 12.41 | 9.73 | 5.22 | 2.33 | 1.36 | 12.77 | 10.32 | 5.21 |
| 3.50 | 1.48 | 17.83 | 13.73 | 7.75 | 2.51 | 1.38 | 14.32 | 11.38 | 5.89 |
| 4.03 | 1.52 | 19.92 | 14.92 | 8.38 | 2.95 | 1.38 | 16.03 | 12.52 | 6.74 |
| 4.47 | 1.55 | 21.29 | 15.92 | 9.05 | 3.79 | 1.48 | 17.08 | 13.46 | 7.19 |
| 4.56 | 1.56 | 21.07 | 15.97 | 9.14 | 4.42 | 1.52 | 20.47 | 15.61 | 8.62 |
| 5.56 | 1.62 | 23.44 | 17.64 | 9.95 | 5.41 | 1.59 | 23.64 | 18.11 | 10.11 |
| 6.37 | 1.68 | 26.11 | 19.89 | 11.32 | 6.92 | 1.68 | 27.40 | 20.81 | 11.69 |
| | | | | | 8.44 | 1.75 | 31.26 | 23.51 | 8.44 |
| | | | | | 9.36 | 1.80 | 32.99 | 24.69 | 9.36 |
| | | | | | 10.74 | 1.87 | 34.96 | 24.59 | 10.74 |
| | | | | | 12.03 | 1.93 | 37.77 | 24.67 | 12.03 |

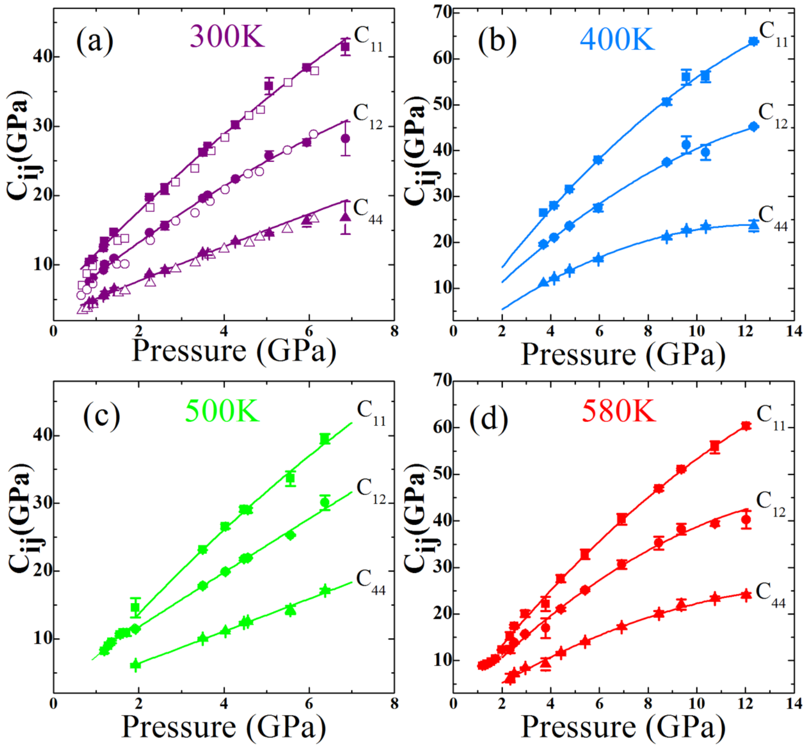

FIG. 6. Representative elastic constants as a function of pressure at (a) 300 K, (b) 400 K, (c) 500 K, and (d) 580 K for $H_2S$ single crystal. Square, circle, and up triangle solid dots represent elastic constants $C_{11}$, $C_{12}$, and $C_{44}$ of this work, and hollow dots are from Shimizu and Sasaki[27] at 300 K. The solid lines represent fitting results with polynomials. At 500 and 580 K, elastic constant $C_{11}$ mutates when the liquid changes to solid phase I.

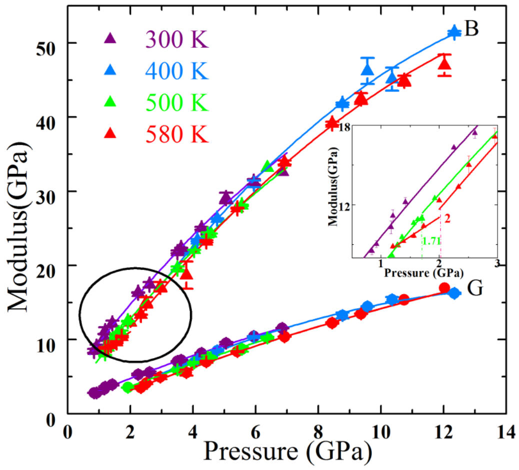

FIG. 7. Bulk (B) and shear (G) moduli variation with pressure at four isotherms for crystalline $H_2S$. The purple, cyan, green, and red solid up triangles and circles represent bulk and shear moduli at 300, 400, 500, and 580 K, respectively. The solid lines represent the polynomial fitting results in Table III. The inset is an enlargement of the drawing circle part.

where $P$ is pressure, $V_0$ is the reference volume at ambient pressure, $V$ is the deformed volume, and $B_0$ and $B'_0$ are the bulk modulus and the first derivative of the bulk modulus respect to pressure at ambient pressure.

The fitting results and uncertainties are listed in Table I. Two EOS fittings give similar curves. Tait EOS fitting shows smaller fitting error; therefore, we choose Tait curves to get arbitrary densities corresponding to the experiment. The isothermal variation of densities with pressure is shown in Fig. 5. We compare the calculated result with the value obtained from XRD at room temperature, and the error is 1.5%. In Table II, we report the calculated density at each $P$-$T$ conditions together with the values of $C_{ij}/\rho$ which do not rely on any assumption on density.

### C. Elastic constants and moduli

With the acquired densities, best fit set of elastic constants and the ($\theta$, $\varphi$, $\chi$) of each plane in the DAC at measured pressure and temperature are defined. Elastic constants as a function of pressure at different temperatures are described in Fig. 6. The elasticity of anisotropic $H_2S$ phase I is fully described by the elastic constants. The calculated elastic constants by using MD fitted densities at 300 K in Fig. 6(a) are in agreement with the results of Shimizu and Sasaki,[27] which meant the fitted densities at 300 K are almost identical with the XRD results of our own and Shimizu and Sasaki.[27] All three isothermal elastic constants enhance dramatically under applied pressure, whereas the elastic constants reveal slight decrease with temperature variation under the same pressure. Among the three elastic constants, $C_{11}$ and $C_{12}$ are more sensitive to the pressure, and the shear constant $C_{44}$ gets a smaller rate of change with pressure. The errors on $C_{ij}$ become bigger because of the decreased intensity and broadened peaks caused by crystal breaking at higher pressure, and the error of bulk modulus also gets bigger at high pressure. Assuming the high temperature density data are correct, the relative accuracy on $C_{ij}$ is within 5%.

Moreover, the isothermal bulk modulus B and shear modulus G as a function of pressure are calculated according to the Voigt–Reuss–Hill averaging method as follows:

$$B = \frac{C_{11} + 2C_{12}}{3}, \tag{6}$$

$$G(Voigt) = \frac{C_{11} - C_{12} + 3C_{44}}{5}, \tag{7}$$

$$G(Reuss) = \frac{5C_{44}(C_{11} - C_{12})}{4C_{44} + 3(C_{11} - C_{12})}, \tag{8}$$

$$G(Hill) = \frac{G(Voigt) + G(Reuss)}{2}. \tag{9}$$

All calculated moduli at different pressure and temperature are presented in Fig. 7. The moduli of $H_2S$ are found to dramatically increase with increasing pressure along the

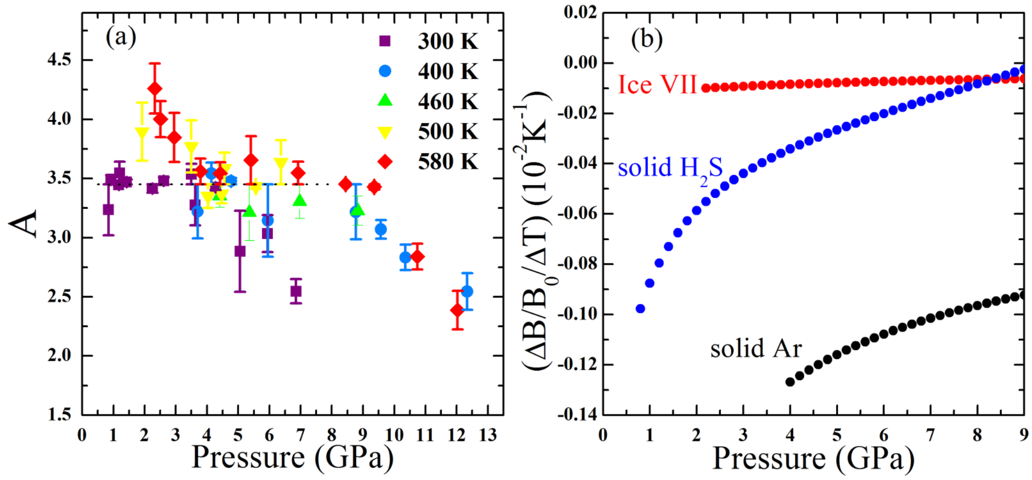

FIG. 8. (a) Elastic anisotropy as a function of pressure at different temperatures. (b) Comparing $\Delta B/B_0$ per 100 K increasing among ice VII, $H_2S$, and argon at different pressures. The isothermal bulk moduli dependence of pressure data of ice VII comes from Shimizu *et al.*[44] and Bezacier *et al.*,[45] and argon is obtained from Brillouin data of Marquardt *et al.*[46] The $\Delta B/B0$ per 100 K represents the relative change between two isotherms in B for every 100 K interval. $B_0$ means the bulk modulus at ambient condition.

TABLE III. The polynomial fitting parameters of moduli and elastic constants as a function of pressure.

| T (K) | B (GPa) | | | G (GPa) | | | $C_{11}$ (GPa) | | | $C_{12}$ (GPa) | | | $C_{44}$ (GPa) | | |
|---|---|---|---|---|---|---|---|---|---|---|---|---|---|---|---|
| | $B^0$ | $B'$ | $B''$ | $G^0$ | $G'$ | $G''$ | $C_{11}^0$ | $C_{11}'$ | $C_{11}''$ | $C_{12}^0$ | $C_{12}'$ | $C_{12}''$ | $C_{44}^0$ | $C_{44}'$ | $C_{44}''$ |
| 300 | 4.07 | 5.73 | −0.18 | 1.34 | 1.81 | −0.05 | 4.6 | 7.19 | −0.25 | 2.91 | 5.93 | −0.31 | 1.82 | 3.4 | −0.17 |
| 400 | 3.61 | 5.59 | −0.14 | 1.14 | 1.72 | 0.034 | 4.33 | 6.28 | −0.12 | 2.8 | 4.84 | −0.11 | 1.66 | 2.73 | −0.06 |
| 500 | 3.26 | 5.41 | −0.17 | 0.83 | 1.65 | −0.03 | 4.03 | 5.66 | 0.041 | 2.55 | 4.89 | −0.14 | 1.44 | 2.63 | −0.05 |
| 580 | 3.04 | 5.36 | −0.14 | 0.71 | 1.55 | −0.02 | 3.76 | 5.4 | −0.04 | 2.22 | 4.59 | −0.12 | 1.27 | 2.66 | −0.06 |

isotherm, but slightly diminish with the elevated temperatures at the same pressure. B presents more sensitive to pressure than G. The slope of B is approximately three times of G. At the same time, we detect the Brillouin signal of the liquid state during 500 and 580 K in the inset figure of Fig. 7. We find that B jumps from 11.21 to 11.52 at 1.71 GPa, 500 K and from 11.05 to 11.68 at 2 GPa, 580 K. Thus, the two high temperature's freezing pressure points and their fall on the extrapolation of the known melting curve are determined. The polynomial fitting $B_0$ is in good agreement with the fitting results of Tait EOS, and the error is about 5%.

The isothermal fitting results of bulk and shear moduli together with three elastic constants as a function of pressure are well represented by quadratic polynomials function (such as $B = B^0 + B' \times P + B'' \times P^2$) and shown in Table III.

## D. Elastic anisotropy

Zener elastic anisotropy (A) for cubic crystals can be defined as: $A = 2C_{44}/(C_{11} - C_{12})$. The anisotropy is insensitive to temperature and pressure change, as shown in Fig. 8(a); firstly, it is stable at an average around 3.45 and then decreases with increasing pressure. The decreased tendency indicates that the elastic anisotropy weakens at high pressure. We define a value $\Delta B/B_0/\Delta T$ to describe the relative change rate in volume for every 100 K rising, as shown in Fig. 8(b). The phenomenon of increase in $\Delta B/B_0/\Delta T$ with elevated pressure is observed in all three compounds, whereas the relative changing rates are not exactly the same. The rate in argon is the smallest one; in other words, when temperature increases by 100 K, argon has the largest relative change of B, which is 3.7 times as much as $H_2S$ and 15 times as much as ice VII. $H_2S$, ice VII, and argon are all cubic structures within a certain pressure-temperature range,[47,48] ice VII and $H_2S$ belong to hydrogen chalcogenide with hydrogen bonds, and argon has similar atomic weight with $H_2S$ but has no H-bonds. We speculate that the considerable difference results from the support of hydrogen-bonds in $H_2S$ and ice VII preventing the change of volume caused by pressure and temperature. $\Delta B/B_0/\Delta T$ in $H_2S$ shows more than three times as large as ice VII at first, which is partly because sulfur hydrogen bonds are more easily to compress than oxygen hydrogen bonds. Besides, at low pressure, the structure of $H_2S$ appears to be unaffected by hydrogen bonding at all, while water is much more strongly H bonded.[19] Upon further compression, hydrogen-bonds in $H_2S$ are significantly enhanced, so the changing rate between ice VII and $H_2S$ becomes consistent. This relative change of B explores the possible overall effect of hydrogen bonds under high *P-T*.

## IV. CONCLUSION

We have performed *in situ* Brillouin scattering studies on single crystal $H_2S$ up to 12 GPa and 580 K for the first time. We systematically discuss the elastic properties' dependence of pressure and temperature. The changes of acoustic velocities and elastic constants together with moduli as a function of pressure are given along four isotherms. Molecular dynamics simulations are integrated with experiments to obtain isothermal equations of state, and well-fitting results are obtained with Tait and third-order Birch-Murnaghan EOS. The hydrogen bonding in $H_2S$ shows an effect of preventing the change of volume caused by pressure and temperature. The phase diagram and melting curve of $H_2S$ have been extended to 580 K.

## ACKNOWLEDGMENTS

The authors are grateful to Sergey N. Tkachev for his help during the experiments. The room temperature *in situ* Brillouin scattering and synchrotron XRD experiments were performed at GeoSoilEnviroCARS (The University of Chicago, Sector 13), Advanced Photon Source (APS), Argonne National Laboratory. GeoSoilEnviroCARS is supported by the National Science Foundation-Earth Sciences (EAR-1634415) and Department of Energy-GeoSciences (DE-FG02-94ER14466). This research used resources of the Advanced Photon Source, a U.S. Department of Energy (DOE) Office of Science User Facility operated for the DOE Office of Science by Argonne National Laboratory under Contract No. DE-AC02-06CH11357. This work was supported by National Key R&D Program of China (No. 2018YFA0305900), National Natural Science Foundation of China (Nos. 51572108, 51632002, 11504127, 51025206, 11274137, and 11474127), the 111 Project (No. B12011), Program for Changjiang Scholars and Innovative Research Team in University (No. IRT1132), and National Found for Fostering Talents of Basic Science (No. J1103202). This work is dedicated to Professor Guangtian Zou on the occasion of his 80th birthday.

[1] D. Duan, F. Tian, Z. He, X. Meng, L. Wang, C. Chen, X. Zhao, B. Liu, and T. Cui, J. Chem. Phys. **133**, 074509 (2010).
[2] H. Wang, J. S. Tse, K. Tanaka, T. Iitaka, and Y. Ma, Proc. Natl. Acad. Sci. U.S.A. **109**, 6463 (2012).
[3] Y. Li, G. Gao, Y. Xie, Y. Ma, T. Cui, and G. Zou, Proc. Natl. Acad. Sci. U.S.A. **107**, 15708 (2010).

[4] A. P. Drozdov, M. I. Eremets, and I. A. Troyan, arXiv:1508.06224 [cond-mat] (2015).
[5] F. Peng, Y. Sun, C. J. Pickard, R. J. Needs, Q. Wu, and Y. Ma, Phys. Rev. Lett. **119**, 107001 (2017).
[6] B. Sakintuna, F. Lamari-Darkrim, and M. Hirscher, Int. J. Hydrogen Energy **32**, 1121 (2007).
[7] W. L. Mao and H. K. Mao, Proc. Natl. Acad. Sci. U.S.A. **101**, 708 (2004).
[8] D. Duan, X. Huang, F. Tian, D. Li, H. Yu, Y. Liu, Y. Ma, B. Liu, and T. Cui, Phys. Rev. B **91**, 180502 (2015).
[9] Y. Li, J. Hao, H. Liu, Y. Li, and Y. Ma, J. Chem. Phys. **140**, 174712 (2014).
[10] A. P. Drozdov, M. I. Eremets, I. A. Troyan, V. Ksenofontov, and S. I. Shylin, Nature **525**, 73 (2015).
[11] X. Huang, X. Wang, D. Duan, B. Sundqvist, X. Li, Y. Huang, F. Li, Q. Zhou, B. Liu, and T. Cui, arXiv:1610.02630 [cond-mat.supr-con] (2016).
[12] L. Gao, Y. Y. Xue, F. Chen, Q. Xiong, R. L. Meng, D. Ramirez, C. W. Chu, J. H. Eggert, and H. K. Mao, Phys. Rev. B **50**, 4260 (1994).
[13] A. F. Goncharov, S. S. Lobanov, I. Kruglov, X.-M. Zhao, X.-J. Chen, A. R. Oganov, Z. Konôpková, and V. B. Prakapenka, Phys. Rev. B **93**, 174105 (2016).
[14] I. Errea, M. Calandra, C. J. Pickard, J. R. Nelson, R. J. Needs, Y. Li, H. Liu, Y. Zhang, Y. Ma, and F. Mauri, Nature **532**, 81 (2016).
[15] Y. Quan and W. E. Pickett, Phys. Rev. B **93**, 104526 (2016).
[16] E. J. Pace, J. Binns, M. P. Alvarez, P. Dalladay-Simpson, E. Gregoryanz, and R. T. Howie, J. Chem. Phys. **147**, 184303 (2017).
[17] D. Duan, Y. Liu, F. Tian, D. Li, X. Huang, Z. Zhao, H. Yu, B. Liu, W. Tian, and T. Cui, Sci. Rep. **4**, 6968 (2014).
[18] E. Sandor and S. O. Ogunade, Nature **224**, 905 (1969).
[19] J. K. Cockcroft and A. N. Fitch, Z. Kristallogr. Crystalline Mater. **193**, 1 (1990).
[20] M. J. Collins, C. I. Ratcliffe, and J. A. Ripmeester, J. Phys. Chem. **93**, 7495 (1989).
[21] H. Shimizu, Y. Nakamichi, and S. Sasaki, J. Chem. Phys. **95**, 2036 (1991).
[22] H. Fujihisa, H. Yamawaki, M. Sakashita, and K. Aoki, Phys. Rev. B **57**, 2651 (1998).
[23] R. Rousseau, M. Boero, M. Bernasconi, M. Parrinello, and K. Terakura, Phys. Rev. Lett. **83**, 2218 (1999).
[24] T. Ikeda, Phys. Rev. B **64**, 104103 (2001).
[25] L. Wang, F. Tian, W. Feng, C. Chen, Z. He, Y. Ma, T. Cui, B. Liu, and G. Zou, J. Chem. Phys. **132**, 164506 (2010).
[26] A. Polian, J. Raman Spectrosc. **34**, 633 (2003).
[27] H. Shimizu and S. Sasaki, Science **257**, 514 (1992).
[28] S. Murase, M. Yanagisawa, S. Sasaki, T. Kume, and H. Shimizu, J. Phys. Condens. Matter **14**, 11537 (2002).
[29] G. Shen, V. B. Prakapenka, P. J. Eng, M. L. Rivers, and S. R. Sutton, J. Synchrotron. Radiat. **12**, 642 (2005).
[30] H. Shimizu, H. Yamaguchi, S. Sasaki, A. Honda, S. Endo, and M. Kobayashi, Phys. Rev. B **51**, 9391 (1995).
[31] H. Fujihisa, H. Yamawaki, M. Sakashita, A. Nakayama, T. Yamada, and K. Aoki, Phys. Rev. B **69**, 214102 (2004).
[32] J. S. Loveday, R. J. Nelmes, S. Klotz, J. M. Besson, and G. Hamel, Phys. Rev. Lett. **85**, 1024 (2000).
[33] A. G. Every, Phys. Rev. Lett. **42**, 1065 (1979).
[34] S. Hiroyasu and S. Shigeo, AIP Conf. Proc. **309**, 89 (1994).
[35] H. Z. Cummins and P. E. Schoen, in *Laser Handbook* (North-Holland Publishing Co., Amsterdam, 1972), p. 1030.
[36] G. Kresse and J. Hafner, Phys. Rev. B **48**, 13115 (1993).
[37] E. R. Hernandez, A. Rodriguez-Prieto, A. Bergara, and D. Alfe, Phys. Rev. Lett. **104**, 185701 (2010).
[38] G. Kresse and J. Furthmüller, Phys. Rev. B **54**, 11169 (1996).
[39] P. E. Blöchl, Phys. Rev. B **50**, 17953 (1994).
[40] G. Kresse and D. Joubert, Phys. Rev. B **59**, 1758 (1999).
[41] J. P. Perdew, K. Burke, and M. Ernzerhof, Phys. Rev. Lett. **77**, 3865 (1996).
[42] H. J. Monkhorst and J. D. Pack, Phys. Rev. B **13**, 5188 (1976).
[43] E. Hernández, J. Chem. Phys. **115**, 10282 (2001).
[44] H. Shimizu, T. Nabetani, T. Nishiba, and S. Sasaki, Phys. Rev. B **53**, 6107 (1996).
[45] L. Bezacier, B. Journaux, J. P. Perrillat, H. Cardon, M. Hanfland, and I. Daniel, J. Chem. Phys. **141**, 104505 (2014).
[46] H. Marquardt, S. Speziale, A. Gleason, S. Sinogeikin, I. Kantor, and V. B. Prakapenka, J. Appl. Phys. **114**, 093517 (2013).
[47] S. Klotz, K. Komatsu, H. Kagi, K. Kunc, A. Sano-Furukawa, S. Machida, and T. Hattori, Phys. Rev. B **95**, 17411 (2017).
[48] F. Datchi, P. Loubeyre, and R. L. Toullec, Phys. Rev. B **61**, 6535 (2000).